Mathematical Models and Methods in Applied Sciences
Vol. 20, No. 11 (2010) 2075–2107

DOI: 10.1142/S0218202510004878

World Scientific
www.worldscientific.com

ISOGEOMETRIC COLLOCATION METHODS

F. AURICCHIO[*,¶], L. BEIRÃO DA VEIGA[†],
T. J. R. HUGHES[‡], A. REALI[*,‖] and G. SANGALLI[§]

[*]*Structural Mechanics Department,*
University of Pavia

[†]*Mathematics Department "F. Enriques",*
University of Milan

[‡]*Institute for Computational Engineering and Sciences,*
University of Texas at Austin

[§]*Mathematics Department, University of Pavia*
[¶]*auricchio@unipv.it*
[‖]*alessandro.reali@unipv.it*
[†]*lourenco.beirao@unimi.it*
[‡]*hughes@ices.utexas.edu*
[§]*giancarlo.sangalli@unipv.it*

Received 22 October 2009
Revised 12 February 2010
Communicated by F. Brezzi

We initiate the study of collocation methods for NURBS-based isogeometric analysis. The idea is to connect the superior accuracy and smoothness of NURBS basis functions with the low computational cost of collocation. We develop a one-dimensional theoretical analysis, and perform numerical tests in one, two and three dimensions. The numerical results obtained confirm theoretical results and illustrate the potential of the methodology.

Keywords: Isogeometric analysis; collocation methods; non-uniform rational B-splines.

AMS Subject Classification: 22E46, 53C35, 57S20

1. Introduction

Isogeometric analysis is a computational mechanics technology based on functions used to represent geometry.[1,4–8,10–12,19,20,27,30] The idea is to build a geometry model and, rather than develop a finite element model approximating the geometry, to directly use the functions describing the geometry in analysis.

In Computer-Aided Design (CAD) systems used in engineering, Non-Uniform Rational B-Splines (NURBS) are the dominant technology. When a NURBS model is constructed, the basis functions used to define the geometry can be systematically enriched by *h*-, *p*-, or *k*-refinement (i.e. smooth order elevation; see Cottrell *et al.*[12])

without altering the geometry or its parametrization. This means that adaptive mesh refinement techniques can be utilized without a link to the CAD database, in contrast with finite element methods. This appears to be a distinct advantage of isogeometric analysis over finite element analysis. In addition, on a per-degree-of-freedom basis, isogeometric analysis exhibits superior accuracy and robustness compared with finite element analysis.[1,8,9,20] This is particularly true when a k-refined basis is adopted. In this case, the upper part of the discrete spectrum is better behaved,[20] resulting in better conditioned discrete systems. Therefore, isogeometric analysis appears to offer several important advantages over classical finite element analysis.

However, the use of high-degree basis function, as in k-refinement, raises the issue of an efficient implementation. Until now, isogeometric analysis has been implemented by Galerkin formulations. In this case, the efficiency issue is related to the numerical quadrature rules which are adopted when assembling the system of equations. While elementwise Gauss quadrature is optimal in the finite element context, it is sub-optimal when k-refined isogeometric discretizations of Galerkin type are considered. More efficient special rules have been derived for isogeometric analysis by Hughes *et al.*[21] Taking inspiration from that work, we initiate here the study of even more efficient collocation-based methods.

The structure of the paper is the following. In Sec. 2, we present a brief review of NURBS and isogeometric analysis, and we introduce the proposed collocation scheme. In Sec. 3, we develop a one-dimensional theoretical analysis of the method, which serves the dual purpose of providing theoretical background and guiding the selection of collocation points. In Sec. 4, we present numerical tests on simple elliptic problems, in one, two and three dimensions. We test the accuracy of the method, study the behavior of the discrete eigenspectrum and discuss the performance of the scheme with respect to the choice of collocation points. Finally, in Sec. 5, we present an analytical cost comparison between the isogeometric Galerkin method and the isogeometric collocation scheme. We draw conclusions in Sec. 6.

2. NURBS-Based Isogeometric Analysis

Non-Uniform Rational B-Splines (NURBS) are a standard tool for describing and modeling curves and surfaces in computer-aided design and computer graphics (see Piegl and Tiller[25] and Rogers[28] for an extensive description of these functions and their properties). In this work, we use NURBS as an analysis tool, as proposed by Hughes *et al.*[19] The aim of this section is to present a short description of B-splines and NURBS, followed by a simple discussion on the basics of isogeometric analysis and by an introduction to the proposed collocation method.

2.1. *B-splines and NURBS*

B-splines in the plane are piecewise polynomial curves composed of linear combinations of B-spline basis functions. The coefficients ($\mathbf{B}_i$) are points in the plane, referred to as *control points*.

A *knot vector* is a set of non-decreasing real numbers representing coordinates in the parametric space of the curve

$$\{\xi_1 = 0, \ldots, \xi_{n+p+1} = 1\}, \tag{2.1}$$

where p is the order of the B-spline and n is the number of basis functions (and control points) necessary to describe it. The interval $[\xi_1, \xi_{n+p+1}]$ is called a *patch*. A knot vector is said to be *uniform* if its knots are uniformly-spaced and *non-uniform* otherwise; it is said to be *open* if its first and last knots have multiplicity $p+1$. In what follows, we always employ open knot vectors. Basis functions formed from open knot vectors are interpolatory at the ends of the parametric interval $[0, 1]$ but are not, in general, interpolatory at interior knots.

Given a knot vector, univariate B-spline basis functions are defined recursively starting with $p = 0$ (piecewise constants)

$$N_{i,0}(\xi) = \begin{cases} 1 & \text{if } \xi_i \le \xi < \xi_{i+1} \\ 0 & \text{otherwise.} \end{cases} \tag{2.2}$$

For $p > 1$:

$$N_{i,p}(\xi) = \begin{cases} \dfrac{\xi - \xi_i}{\xi_{i+p} - \xi_i} N_{i,p-1}(\xi) + \dfrac{\xi_{i+p+1} - \xi}{\xi_{i+p+1} - \xi_{i+1}} N_{i+1,p-1}(\xi) & \text{if } \xi_i \le \xi < \xi_{i+p+1} \\ 0 & \text{otherwise,} \end{cases} \tag{2.3}$$

where, in (2.3), we adopt the convention $0/0 = 0$.

In Fig. 1 we present an example consisting of $n = 9$ cubic basis functions generated from the open knot vector $\{0, 0, 0, 0, 1/6, 1/3, 1/2, 2/3, 5/6, 1, 1, 1, 1\}$.

If internal knots are not repeated, B-spline basis functions are C^{p-1}-continuous. If a knot has multiplicity k, the basis is C^{p-k}-continuous at that knot. In particular, when a knot has multiplicity p, the basis is C^0 and interpolates the control point at

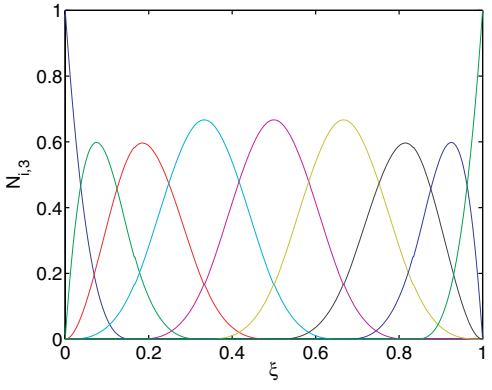

Fig. 1. Cubic basis functions formed from the open knot vector $\{0, 0, 0, 0, 1/6, 1/3, 1/2, 2/3, 5/6, 1, 1, 1, 1\}$.

that location. We define

$$\hat{\mathcal{S}}_n = \text{span}\{N_{i,p}(\xi), i = 1, \ldots, n\}. \tag{2.4}$$

By means of tensor products, a multi-dimensional B-spline region can be constructed. We discuss here the case of a two-dimensional region, the higher-dimensional case being analogous. Consider the knot vectors $\{\xi_1 = 0, \ldots, \xi_{n+p+1} = 1\}$ and $\{\eta_1 = 0, \ldots, \eta_{m+q+1} = 1\}$, and an $n \times m$ net of control points $\mathbf{B}_{i,j}$. One-dimensional basis functions $N_{i,p}$ and $M_{j,q}$ (with $i = 1, \ldots, n$ and $j = 1, \ldots, m$) of order p and q, respectively, are defined from the knot vectors, and the B-spline region is the image of the map $\mathbf{S} : [0,1] \times [0,1] \to \bar{\Omega}$ given by

$$\mathbf{S}(\xi, \eta) = \sum_{i=1}^{n} \sum_{j=1}^{m} N_{i,p}(\xi) M_{j,q}(\eta) \mathbf{B}_{i,j}. \tag{2.5}$$

The two-dimensional parametric space is the domain $[0,1] \times [0,1]$. Observe that the two knot vectors $\{\xi_1 = 0, \ldots, \xi_{n+p+1} = 1\}$ and $\{\eta_1 = 0, \ldots, \eta_{m+q+1} = 1\}$ generate a mesh of rectangular elements in the parametric space in a natural way. Analogous to (2.4), we define

$$\hat{\mathcal{S}}_{nm} = \text{span}\{N_{i,p}(\xi) M_{j,q}(\eta), i = 1, \ldots, n,\ j = 1, \ldots, m\}. \tag{2.6}$$

In general, a rational B-spline in $\mathbb{R}^d$ is the projection onto d-dimensional physical space of a polynomial B-spline defined in $(d+1)$-dimensional homogeneous coordinate space. For a complete discussion see the book by Farin[17] and references therein. In this way, a great variety of geometrical entities can be constructed and, in particular, all conic sections in physical space can be obtained exactly. The projective transformation of a B-spline curve yields a rational polynomial curve. Note that when we refer to the "degree" or "order" of a NURBS curve, we mean the degree or order, respectively, of the polynomial curve from which the rational curve was generated.

To obtain a NURBS curve in $\mathbb{R}^2$, we start from a set $\mathbf{B}_i^{\omega} \in \mathbb{R}^3$ $(i = 1, \ldots, n)$ of control points ("projective points") for a B-spline curve in $\mathbb{R}^3$ with knot vector Ξ. Then the control points for the NURBS curve are

$$[\mathbf{B}_i]_k = \frac{[\mathbf{B}_i^{\omega}]_k}{\omega_i}, \quad k = 1, 2, \tag{2.7}$$

where $[\mathbf{B}_i]_k$ is the kth component of the vector $\mathbf{B}_i$ and $\omega_i = [\mathbf{B}_i^{\omega}]_3$ is referred to as the ith *weight*. The NURBS basis functions of order p are then defined as

$$R_i^p(\xi) = \frac{N_{i,p}(\xi)\omega_i}{\sum_{\hat{i}=1}^{n} N_{\hat{i},p}(\xi)\omega_{\hat{i}}}. \tag{2.8}$$

The NURBS curve is defined by

$$\mathbf{C}(\xi) = \sum_{i=1}^{n} R_i^p(\xi) \mathbf{B}_i. \tag{2.9}$$

Analogously to B-splines, NURBS basis functions on the two-dimensional parametric space $\hat{\Omega} = [0,1] \times [0,1]$ are defined as

$$R_{i,j}^{p,q}(\xi,\eta) = \frac{N_{i,p}(\xi) M_{j,q}(\eta) \omega_{i,j}}{\sum_{\hat{i}=1}^{n} \sum_{\hat{j}=1}^{m} N_{\hat{i},p}(\xi) M_{\hat{j},q}(\eta) \omega_{\hat{i},\hat{j}}}, \tag{2.10}$$

where $\omega_{i,j} = (\mathbf{B}_{i,j}^{\omega})_3$. Observe that the continuity and support of NURBS basis functions are the same as for B-splines.

NURBS regions, similarly to B-spline regions, are defined in terms of the basis functions (2.10). In particular, we assume from now on that the physical domain Ω is a NURBS region associated with the $n \times m$ net of control points $\mathbf{B}_{i,j}$, and we introduce the geometrical map $\mathbf{F} : \hat{\Omega} \to \bar{\Omega}$ given by

$$\mathbf{F}(\xi,\eta) = \sum_{i=1}^{n} \sum_{j=1}^{m} R_{i,j}^{p,q}(\xi,\eta) \mathbf{B}_{i,j}. \tag{2.11}$$

For the sake of simplicity, the extension to three (or more) dimensions is not discussed here (but it is completely analogous).

2.2. *Basics of isogeometric analysis*

In one-space dimension, let F be the parametrization of the physical interval $[a,b]$, which is assumed piecewise smooth with piecewise smooth inverse. Following the isoparametric approach, the space of NURBS functions on $[a,b]$ is defined as the span of the *push-forward* of the basis functions (2.8)

$$\mathcal{V}_n = \operatorname{span}\{R_i^p \circ F^{-1},\ i = 1,\dots,n\}. \tag{2.12}$$

Similarly, in two dimensions, let $\mathbf{F}$ be the parametrization of the physical domain Ω, as given in (2.11). We assume that the Jacobian of $\mathbf{F}$ and its inverse are non-singular. The image of the elements in the parametric space are elements in the physical space. The physical mesh is therefore made of elements $\mathbf{F}((\xi_i,\xi_{i+1}) \times (\eta_j,\eta_{j+1}))$, with $i = 1,\dots,n+p$, $j = 1,\dots,m+q$. We denote by h the mesh-size, that is, the maximum diameter of the elements of the physical mesh.

Again, the space of NURBS functions on Ω is defined as the span of the *push-forward* of the basis functions (2.10)

$$\mathcal{V}_{nm} = \operatorname{span}\{R_{i,j}^{p,q} \circ \mathbf{F}^{-1}, \text{with } i = 1,\dots,n; j = 1,\dots,m\}. \tag{2.13}$$

The numerical solution of a boundary-value problem is sought in the space $\mathcal{V}_n$ or $\mathcal{V}_{nm}$, endowed with suitable boundary conditions.

The interested reader may find more details on isogeometric analysis as well as many interesting applications in a number of recently published papers.[6,11,12,10,19,27]

2.3. *Isogeometric collocation method*

In the first part of this section we present the concept of isogeometric collocation method in a general setting, while in the second part we give a more detailed description for a particular case.

Consider the following boundary-value problem

$$\begin{cases} \mathcal{D}u = f & \text{in } \Omega, \\ \mathcal{G}u = \mathbf{g} & \text{on } \partial\Omega, \end{cases} \tag{2.14}$$

where the solution $u : \Omega \to \mathbb{R}$, $\mathcal{D}$ represents a scalar differential operator, $\mathcal{G}u : \partial\Omega \to \mathbb{R}^r$ is a vector operator ($r \in \mathbb{N}^+$) representing boundary conditions, and $f, \mathbf{g}$ are given data. Note that both operators $\mathcal{D}$ and $\mathcal{G}$ may depend on the position $x \in \Omega \cup \partial\Omega$.

We introduce a finite set of collocation points $\{\hat{\tau}_\vartheta\}_{\vartheta\in\mathcal{I}}$ in $\hat{\Omega} = [0,1] \times [0,1]$, divided into two distinct sets $\mathcal{I}_\mathcal{D}$ and $\mathcal{I}_\mathcal{G}$, such that $\mathcal{I} = \mathcal{I}_\mathcal{D} \cup \mathcal{I}_\mathcal{G}$, and

$$\vartheta \in \mathcal{I}_\mathcal{G} \Rightarrow \hat{\tau}_\vartheta \in \partial\hat{\Omega}, \quad \#\mathcal{I}_\mathcal{D} + r \cdot \#\mathcal{I}_\mathcal{G} = \dim(\mathcal{V}_{nm}),$$

where # indicates the cardinality of a set. Note that the collocation points $\hat{\tau}_\vartheta$ are typically built in a tensor product fashion. The choice of the collocation points is crucial for the stability and good behavior of the discrete problem. Finally let $\tau_\vartheta = \mathbf{F}(\hat{\tau}_\vartheta)$, for all $\vartheta \in \mathcal{I}$.

Then, the isogeometric collocation approximation of (2.14) reads: find $u_{nm} \in \mathcal{V}_{nm}$ such that

$$\begin{cases} \mathcal{D}u_{nm}(\tau_\vartheta) = f(\tau_\vartheta) & \forall\, \vartheta \in \mathcal{I}_\mathcal{D}, \\ \mathcal{G}u_{nm}(\tau_\vartheta) = \mathbf{g}(\tau_\vartheta) & \forall\, \vartheta \in \mathcal{I}_\mathcal{G}. \end{cases} \tag{2.15}$$

As a particular example, we consider the case where the collocation points are chosen using the Greville abscissae[14,15] of the knot vectors. To simplify the presentation, we restrict our description to the case of a second-order operator, still indicated by $\mathcal{D}$, with boundary conditions represented by the scalar operator $\mathcal{G}u : \partial\Omega \to \mathbb{R}$.

Let $\bar{\xi}_i$, $i = 1, \ldots, n$, be the Greville abscissae related to the knot vector $\{\xi_1, \ldots, \xi_{n+p+1}\}$:

$$\bar{\xi}_i = \frac{\xi_{i+1} + \xi_{i+2} + \cdots + \xi_{i+p}}{p}. \tag{2.16}$$

Analogously, let $\bar{\eta}_j$, $j = 1, \ldots, m$, be the Greville abscissae related to the knot vector $\{\eta_1, \ldots, \eta_{m+q+1}\}$. It is easy to see that $\bar{\xi}_1 = \bar{\eta}_1 = 0$, $\bar{\xi}_n = \bar{\eta}_m = 1$, while all the remaining points are in $(0,1)$. We define the collocation points $\tau_{ij} \in \Omega$ by the tensor product structure

$$\tau_{ij} = \mathbf{F}(\hat{\tau}_{ij}), \quad \hat{\tau}_{ij} = (\bar{\xi}_i, \bar{\eta}_j) \in \hat{\Omega},$$

for $i = 1, \ldots, n$, $j = 1, \ldots, m$.

Then, the isogeometric collocation problem with Greville abscissae reads: find $u_{nm} \in \mathcal{V}_{nm}$ such that

$$\begin{cases} \mathcal{D}u_{nm}(\tau_{ij}) = f(\tau_{ij}) & i = 2, \dots, n-1, \;\; j = 2, \dots, m-1, \\ \mathcal{G}u_{nm}(\tau_{ij}) = g(\tau_{ij}) & (i,j) \in \{1,n\} \times \{1, \dots, m\} \cup \{1, \dots, n\} \times \{1,m\}. \end{cases} \tag{2.17}$$

We wish to remark that collocating at Greville abscissae as in the example above is just one of the possible options. In the following, we will also consider a couple of other interesting choices (see Sec. 3.3).

3. Theoretical Analysis

This section is devoted to the theoretical analysis of the NURBS-based collocation approach. We first present an abstract framework, which is based on the results of De Boor and Swartz.[13] Within this framework, we then present a theoretical analysis of the one-dimensional model problem. Finally, we discuss the difficulties that are encountered in the theoretical analysis of the multi-dimensional case.

Given any $A, B \in \mathbb{R}$, we write $A \lesssim B$ whenever $A \leq CB$ with the positive constant C depending only on the problem data. We define the symbol $\gtrsim$ analogously, and write $A \simeq B$ whenever both $A \lesssim B$ and $A \gtrsim B$ hold, in general with different constants.

3.1. *The abstract problem and its discretization*

Taking the initial steps from De Boor and Swartz,[13] the main idea of the proof is to rewrite the differential operator (of order n) $\mathcal{D}$ as a perturbation of the nth derivative operator. As it will be clearer in the following, this can be achieved using a Green function.[13]

Given a Banach space $\mathcal{W}$, endowed with the norm $\|\cdot\|_{\mathcal{W}}$, a linear operator $T : \mathcal{W} \to \mathcal{W}$, and datum $\psi \in \mathcal{W}$, we consider the following abstract problem: Find $y \in \mathcal{W}$ such that

$$(I + T)y = \psi. \tag{3.1}$$

The following assumption of well-posedness is made.

Assumption 3.1. There exists one and only one solution to problem (3.1) and

$$\|(I + T)z\|_{\mathcal{W}} \simeq \|z\|_{\mathcal{W}} \quad \forall\, z \in \mathcal{W}. \tag{3.2}$$

Observe that (3.2) implies the continuity of T. In consideration of the eventual discretization of (3.1), we also require the next assumption.

Assumption 3.2. T is compact, and in particular there exists a compact subspace $\mathcal{W}^+$ of $\mathcal{W}$ such that T is continuous from $\mathcal{W}$ to $\mathcal{W}^+$, that is, $\|Tz\|_{\mathcal{W}^+} \lesssim \|z\|_{\mathcal{W}}\ \forall\, z \in \mathcal{W}$.

Given an n-dimensional space $\mathcal{W}_n \subset \mathcal{W}$, and a linear projector $Q_n : \mathcal{W} \to \mathcal{W}_n$, we consider the following discretization of (3.1): Find $y_n \in \mathcal{W}_n$ such that

$$Q_n(I + T)y_n = Q_n\psi. \tag{3.3}$$

Observe that $Q_n(I+T)y_n = y_n + Q_nTy_n$. In the following sections the operator Q_n will denote interpolation. We make the following two assumptions on Q_n and $\mathcal{W}_n$.

Assumption 3.3. There exists a constant $C_s > 0$, independent of n, such that $\|Q_n z\|_{\mathcal{W}} \leq C_s \|z\|_{\mathcal{W}}$, for all $z \in \mathcal{W}$.

Assumption 3.4. With the notation of Assumption 3.2,

$$\min_{z_n \in \mathcal{W}_n} \|z - z_n\|_{\mathcal{W}} \leq c_n \|z\|_{\mathcal{W}^+} \quad \forall\, z \in \mathcal{W}^+, \tag{3.4}$$

and the positive constants $c_n \to 0$ as $n \to \infty$.

With these assumptions we have the following result.

Lemma 3.1. *There exists $\bar{n} \in \mathbb{N}$, depending only on the operator T and the problem datum ψ, such that the operator $(I + Q_nT) : \mathcal{W} \to \mathcal{W}$ is an isomorphism for all $n \geq \bar{n}$. Moreover, for $n \geq \bar{n}$*

$$\|(I + Q_nT)z\|_{\mathcal{W}} \simeq \|z\|_{\mathcal{W}} \quad \forall\, z \in \mathcal{W}. \tag{3.5}$$

Proof. Let $z \in \mathcal{W}$. Adding and subtracting any $z_n \in \mathcal{W}_n$, using that $Q_n z_n = z_n$ and the continuity of Q_n gives

$$\begin{aligned} \|(I - Q_n)z\|_{\mathcal{W}} &\leq \|z - z_n\|_{\mathcal{W}} + \|z_n - Q_n z\|_{\mathcal{W}} \\ &= \|z - z_n\|_{\mathcal{W}} + \|Q_n(z - z_n)\|_{\mathcal{W}} \\ &\leq (1 + C_s)\|z - z_n\|_{\mathcal{W}}. \end{aligned} \tag{3.6}$$

Selecting z_n to be the minimizer in (3.4), the above bound gives

$$\|(I - Q_n)z\|_{\mathcal{W}} \leq (1 + C_s)c_n \|z\|_{\mathcal{W}^+}. \tag{3.7}$$

Adding and subtracting Tz, using the triangle inequality, and applying (3.7) yields

$$\begin{aligned} \|(I + Q_nT)z\|_{\mathcal{W}} &\leq \|(I + T)z\|_{\mathcal{W}} + \|(I - Q_n)Tz\|_{\mathcal{W}} \\ &\leq \|(I + T)z\|_{\mathcal{W}} + (1 + C_s)c_n \|Tz\|_{\mathcal{W}^+}. \end{aligned} \tag{3.8}$$

Bound (3.8) combined with (3.2) and Assumption 3.2 gives

$$\|(I + Q_nT)z\|_{\mathcal{W}} \lesssim \|z\|_{\mathcal{W}} + (1 + C_s)c_n \|z\|_{\mathcal{W}}, \tag{3.9}$$

which, due to Assumption 3.4, gives

$$\|(I + Q_nT)z\|_{\mathcal{W}} \lesssim \|z\|_{\mathcal{W}}. \tag{3.10}$$

Very similar steps as the ones above give

$$\|(I + Q_nT)z\|_{\mathcal{W}} \gtrsim \|z\|_{\mathcal{W}} - (1 + C_s)c_n \|z\|_{\mathcal{W}}, \tag{3.11}$$

which for n sufficiently large yields

$$\|(I + Q_nT)z\|_{\mathcal{W}} \gtrsim \|z\|_{\mathcal{W}}. \tag{3.12}$$

Bound (3.5) is proved by (3.10) and (3.12). □

Therefore, the operator $(I + Q_n T)$ is one-to-one and its restriction $(I + Q_n T) : \mathcal{W}_n \to \mathcal{W}_n$ is an isomorphism. The following corollary is immediate.

Corollary 3.1. *For $n \geq \bar{n}$, Problem (3.3) has a unique solution.*

We can now derive the main result of this section.

Proposition 3.1. *Let Assumptions 3.1–3.4 hold. Let y be the solution of (3.1) and y_n the solution of (3.3). Then*

$$\|y - y_n\|_{\mathcal{W}} \lesssim (1 + C_s) \min_{z_n \in \mathcal{W}_n} \|y - z_n\|_{\mathcal{W}}$$

for all n sufficiently large.

Proof. Applying the operator Q_n to both sides of (3.1) and subtracting (3.3), it follows that

$$Q_n(I + T)(y - y_n) = 0. \tag{3.13}$$

First using Lemma 3.1, then applying (3.13) we infer

$$\|y - y_n\|_{\mathcal{W}} \lesssim \|(I + Q_n T)(y - y_n)\|_{\mathcal{W}} = \|(I - Q_n)(y - y_n)\|_{\mathcal{W}}. \tag{3.14}$$

From (3.14), noting that $Q_n y_n = y_n$ and using (3.6), we get

$$\|y - y_n\|_{\mathcal{W}} \lesssim \|(I - Q_n)y\|_{\mathcal{W}} \leq (1 + C_s) \min_{z_n \in \mathcal{W}_n} \|y - z_n\|_{\mathcal{W}}. \tag{3.15}$$

□

3.2. *Theoretical analysis in one dimension*

In this section we restrict our attention to the one-dimensional case of a second-order differential equation and prove that, if the collocation points are chosen suitably, the collocation method converges with optimal rate.

3.2.1. *The continuous problem*

Let f, a_0, a_1, be real functions in $C^0[a, b]$, with $a < b$ given real numbers. Let $g_0, g_1 \in \mathbb{R}$ be scalars and $\mathcal{BC}_0, \mathcal{BC}_1 : C^1[a, b] \to \mathbb{R}$ be linear operators. We are interested in the following one-dimensional ordinary differential equation. Find a real function $u \in C^2[a, b]$ such that

$$\begin{cases} u''(x) + a_1(x)u'(x) + a_0(x)u(x) = f(x) & \forall\, x \in (a, b) \\ \mathcal{BC}_i(u) = g_i & i = 1, 2, \end{cases} \tag{3.16}$$

where u', u'' represent the first and second derivatives of u, respectively. We will indicate the derivative operator of order i also as D^i, $i \in \mathbb{N}$. We assume that (3.16) has one and only one solution u, and that the boundary condition operators $\mathcal{BC}_i$ are linearly independent on $\mathrm{Ker}(D^2)$, that is, on the space of linear functions.

Under this assumption, the Green's function $H_0 : [a, b] \times [a, b] \to \mathbb{R}$ is well defined for the problem $D^2 v = \phi$ with datum $\phi \in C^0[a, b]$ and the homogeneous boundary

conditions $\mathcal{BC}_i(v) = 0$, $i = 1, 2$. As a consequence, all elements of the space

$$C^2_{BC} = \{v \in C^2[a,b] \mid \mathcal{BC}_i(v) = g_i \text{ for } i = 1, 2\}$$

can be written uniquely as

$$v(x) = u_0(x) + \int_a^b H_0(x,t) D^2 v(t) \mathrm{d}t, \tag{3.17}$$

where u_0 is the unique linear function on $[a,b]$ which satisfies $\mathcal{BC}_i(u_0) = g_i$, $i = 1, 2$.

Introducing the partial derivatives of H_0

$$H_k(x,t) = \left(\frac{\partial}{\partial x}\right)^k H_0(x,t) \quad \forall\, (x,t) \in [a,b] \times [a,b], \quad k = 1, 2,$$

and defining $y = D^2 u$, using (3.17) one gets

$$D^k u(x) = D^k u_0(x) + \int_a^b H_k(x,t) y(t) \mathrm{d}t \quad \forall\, x \in [a,b], \quad k = 0, 1, 2. \tag{3.18}$$

Introducing the operator $T : C^0[a,b] \to C^0[a,b]$ as

$$Tz(x) = \sum_{i=0}^{1} a_i(x) \int_a^b H_i(x,t) z(t) \mathrm{d}t \quad \forall\, z \in C^0[a,b], \quad x \in [a,b], \tag{3.19}$$

and defining $\psi \in C^0[a,b]$ as

$$\psi(x) = f(x) - \sum_{i=0}^{1} a_i(x) D^i u_0(x) \quad \forall\, x \in [a,b], \tag{3.20}$$

the problem (3.16) can then be rewritten in the abstract framework of the previous section: substituting (3.18) into (3.16), and using the definitions (3.19)−(3.20), we obtain the problem of finding $y \in C^0[a,b]$ such that

$$(I + T) y = \psi. \tag{3.21}$$

Indeed, the new problem (3.21) is by construction equivalent to Problem (3.16) up to the transformations

$$u = u_0 + \int_a^b H_0(\cdot, t) y(t) \mathrm{d}t, \quad y = D^2 u.$$

For the analysis of (3.16) we select the C^0-topology. We will denote by $\|\cdot\|_{C^0} = \|\cdot\|_{L^\infty}$ the usual L^∞-norm and by

$$|\cdot|_{W^{i,\infty}} = \|D^i \cdot\|_{L^\infty},$$

$$\|\cdot\|_{W^{k,\infty}} = \sum_{i=0}^{k} \|D^i \cdot\|_{L^\infty},$$

the usual Sobolev seminorms and norms. Having the correspondence

$$\mathcal{W} = C^0[a,b] = \{D^2 v \,|\, v \in C^2[a,b],\, v(a) = v(b) = 0\}, \tag{3.22}$$

Assumption 3.1 is equivalent to the well-posedness of (3.16): given $f \in C^0[a,b]$ there exists a unique solution $u \in C^2[a,b]$ to (3.16), with continuous dependence. This is assumed to hold true. Furthermore, Assumption 3.2 is verified, as shown in the next lemma.

Lemma 3.2. *The operator $T : C^0[a,b] \to C^0[a,b]$ in (3.19) is compact. In particular it holds*

$$\|Tz\|_{W^{1,\infty}[a,b]} \lesssim \|z\|_{C^0[a,b]} \quad \forall\, z \in C^0[a,b].$$

Proof. Given any $z \in C^0[a,b]$, let $v \in C^2[a,b]$ be given by

$$v = \int_a^b H_0(\cdot, t) z(t) \mathrm{d}t,$$

so that $D^2 v = z$. Note that, due to the homogeneous boundary conditions satisfied by v,

$$\|D^i v\|_{L^\infty[a,b]} \lesssim \|D^2 v\|_{L^\infty[a,b]} \equiv \|D^2 v\|_{C^0[a,b]} \quad i = 0, 1, 2. \tag{3.23}$$

We then easily have, by definition of T, v and using (3.23)

$$\begin{aligned} \|Tz\|_{W^{1,\infty}[a,b]} &= \left\| \sum_{i=0}^{1} a_i D^i v \right\|_{W^{1,\infty}[a,b]} \\ &\lesssim \sum_{i=0}^{1} \|D^i v\|_{W^{1,\infty}[a,b]} \\ &\lesssim \|D^2 v\|_{C^0[a,b]} = \|z\|_{C^0[a,b]}. \end{aligned} \tag{3.24}$$

Finally, the compactness of the operator follows from the compact inclusion of $W^{1,\infty}[a,b]$ into $L^\infty[a,b]$. □

3.3. *The discretized differential problem*

Given $n \in \mathbb{N}$, let $\mathcal{V}_{n+2} \subset C^2[a,b]$ be a NURBS space of dimension $n+2$ on the interval $[a,b]$, associated with a spline space $\hat{\mathcal{S}}_{n+2} \subset C^2[0,1]$ on the parametric interval $[0,1]$. Recalling the standard assumptions on the one-dimensional geometrical map F of Sec. 2.2, we now consider $DF > 0$ on the parametric domain $[0,1]$. Given for all $n \in \mathbb{N}$, $\tau_1 < \tau_2 < \cdots < \tau_n$ assigned collocation points in $[a,b]$, we consider the following discrete problem: Find $u_n \in \mathcal{V}_{n+2}$ such that

$$\begin{cases} u_n''(\tau_j) + a_1(\tau_j) u_n'(\tau_j) + a_0(\tau_j) u_n(\tau_j) = f(\tau_j) & j = 1, \ldots, n \\ \mathcal{BC}_i u_n = g_i & i = 1, 2. \end{cases} \tag{3.25}$$

Notice that in one dimension the boundary conditions are imposed exactly by the collocation scheme. Following the notation of the abstract setting presented in Sec. 3.1, we now denote as $\mathcal{W}_n$ the space

$$\mathcal{W}_n = \{D^2 v_n \,|\, v_n \in \mathcal{V}_{n+2},\ v(a) = v(b) = 0\}, \tag{3.26}$$

which is n-dimensional.

Remark 3.1. Since the isoparametric paradigm (2.13) is applied for the construction of $\mathcal{V}_{n+2}$, it follows that the space of global linear polynomials is contained in $\mathcal{V}_{n+2}$. As this subspace is the kernel of the operator D^2, the space $\mathcal{W}_n$ can equivalently be written as

$$\mathcal{W}_n = \{D^2 v_n \,|\, v_n \in \mathcal{V}_{n+2}\}.$$

For the continuous differential problem it is easy to see that the above discrete problem is equivalent to finding $y_n \in \mathcal{W}_n$ such that

$$[(I + T)y_n](\tau_j) = \psi(\tau_j) \quad j = 1, \ldots, n \tag{3.27}$$

up to the transformations

$$u_n = u_0 + \int_a^b H_0(\cdot, t) y_n(t) \mathrm{d}t, \quad y_n = D^2 u_n,$$

where u_0 is, as in (3.17), the linear lifting of the boundary conditions.

Problem (3.25) is what is solved in practice, while problem (3.27) is what we use for the theoretical analysis of the method. Denoting by $Q_n : C^0[a, b] \to \mathcal{W}_n$ the interpolation operator

$$(Q_n(z))(\tau_j) = z(\tau_j) \quad \forall\, z \in C^0[a, b], \quad j = 1, \ldots, n,$$

problem (3.27) fits within the framework of Sec. 3.1. Then, the optimality of the collocation scheme (3.25) follows from Proposition 3.1, if Assumptions 3.3 and 3.4 hold true. The approximation properties of NURBS spaces with respect to the mesh-size h have been studied, in the L^2 setting, by Bazilevs *et al.*[6] Assumption 3.4 follows from the analogous result in the L^∞ setting, which is stated in the next proposition.

Theorem 3.1. *There exists a constant $C_a > 0$, dependent on the geometry map F, weight ω, and on the degree p of the NURBS space $\mathcal{V}_n$, such that*

$$\min_{w_n \in \mathcal{W}_n} \|w - w_n\|_{L^\infty[a,b]} \leq C_a h^l \|w\|_{W^{l,\infty}[a,b]}, \quad \forall\, w \in W^{l,\infty}[a, b], \tag{3.28}$$

with $0 \leq l \leq p - 1$.

Proof. A simple extension to the L^∞ setting of the results in Bazilevs *et al.*[6] for the L^2 framework gives

$$\min_{v_n \in \mathcal{V}_{n,0}} \|v'' - v_n''\|_{L^\infty[a,b]} \leq C h^l \|v\|_{W^{l+2,\infty}[a,b]} \quad \forall\, v \in W^{l+2,\infty}[a, b],\ v(a) = v(b) = 0, \tag{3.29}$$

where $\mathcal{V}_{n,0}$ is the subspace of all functions in $\mathcal{V}_{n+2}$ which are zero at a and b. Because of (3.22) and (3.26), any $w \in W^{l,\infty}[a,b]$ can be written as v'' with $v \in W^{l+2,\infty}[a,b]$ and $v(a) = v(b) = 0$. By definition, any $w_n \in \mathcal{W}_n$ can be written as v_n'' with $v_n \in \mathcal{V}_{n,0}$. Therefore, first using the above observations and (3.29), and then, since v is null at the boundaries, a Poincaré inequality, we obtain

$$\begin{aligned}\min_{w_n \in \mathcal{W}_n} \|w - w_n\|_{L^\infty[a,b]} &= \min_{v_n \in \mathcal{V}_{n,0}} \|v'' - v_n''\|_{L^\infty[a,b]} \\ &\le Ch^l \|v\|_{W^{l+2,\infty}[a,b]} \\ &\le Ch^l \|w\|_{W^{l,\infty}[a,b]}. \end{aligned} \tag{3.30}$$

□

Theorem 3.1 implies Assumption 3.4. The following theorem gives sufficient conditions to guarantee the stability of Q_n, for n large enough, i.e. Assumption 3.3.

Theorem 3.2. *Given $\hat{C}_s > 0$, there exists $\bar{n} \in \mathbb{N}$ such that, for any $n > \bar{n}$ the following holds. Let*

$$\hat{\mathcal{T}}_n = \{D^2 s_n \,|\, s_n \in \hat{\mathcal{S}}_{n+2}\} \subset C^0[0,1],$$

which is n-dimensional, and let $\hat{Q}_n : C^0[0,1] \to \hat{\mathcal{T}}_n$ be the interpolation operator on n points $\hat{\tau}_1 < \hat{\tau}_2 < \cdots < \hat{\tau}_n$ in $[0,1]$. Let the stability condition $\|\hat{Q}_n w\|_{L^\infty} \le \hat{C}_s \|w\|_{L^\infty}$, $\forall\, w \in C^0[0,1]$, hold. Then the interpolation operator $Q_n : C^0[a,b] \to \mathcal{W}_n$ associated with the points $\tau_j = F(\hat{\tau}_j)$ is stable, that is $\|Q_n w\|_{L^\infty} \le C_s \|w\|_{L^\infty}$, $\forall\, w \in C^0[a,b]$. The constants $\bar{n}$ and C_s depend only on $\hat{C}_s$ and the geometry parametrization $F : [0,1] \to [a,b]$.

Proof. Let $v = \int_a^b H_0(\cdot,t) w(t) \mathrm{d}t$. Note that by definition $v(a) = v(b) = 0$ and $w = D^2 v$. Then, the interpolation problem on $[a,b]$, that is, the problem of finding $w_n = Q_n w \in \mathcal{W}_n$ such that

$$w_n(\tau_j) = w(\tau_j), \quad 1 \le j \le n,$$

is equivalent to finding $v_n \in \mathcal{V}_n$ such that

$$(D^2 v_n)(\tau_j) = (D^2 v)(\tau_j), \quad 1 \le j \le n, \quad v_n(a) = v_n(b) = 0, \tag{3.31}$$

with $w_n = D^2 v_n$.

Consider the function of $\hat{x} \in [0,1]$

$$s_n(\hat{x}) = v_n(F(\hat{x}))\omega(\hat{x}), \tag{3.32}$$

where $\omega(\hat{x})$ is the denominator in the definition (2.8) of the NURBS, i.e.

$$\omega(\hat{x}) = \sum_{\hat{i}=1}^{n} N_{\hat{i},p}(\hat{x}) \omega_{\hat{i}}. \tag{3.33}$$

Observe that by definition $s_n \in \hat{\mathcal{S}}_{n+2}$, and that $s_n(0) = s_n(1) = 0$.

Now we want to write the interpolation problem (3.31) in terms of s_n. Denoting by $G = F^{-1}$ the inverse of the geometric parametrization F, we have for all $x \in [a, b]$

$$v_n(x) = \frac{s_n(G(x))}{\omega(G(x))}. \tag{3.34}$$

In the following we denote by $\hat{D}^i$ the i-derivative with respect to $\hat{x}$. Computing the derivatives in (3.32) and using a Poincaré inequality yields

$$\|\hat{D}^2 s_n\|_{L^\infty[0,1]} \lesssim \|v_n\|_{W^{2,\infty}(a,b)} \lesssim \|D^2 v_n\|_{L^\infty(a,b)}, \tag{3.35}$$

where the hidden constant in (3.35) depends on F and ω.

Substituting (3.32) in (3.31), using change of variable and the chain rule for derivatives, in (3.34), we get

$$\sum_{i=0}^{2} b_i(\hat{\tau}_j)(\hat{D}^i s_n)(\hat{\tau}_j) = (D^2 v)(\tau_j), \quad 1 \le j \le n \tag{3.36}$$

with suitable factors $b_i(\hat{x})$. In particular, the leading coefficient is

$$b_2(\hat{x}) = \frac{(DG(F(\hat{x})))^2}{\omega(\hat{x})}.$$

Due to the assumption that $\hat{D}F(\hat{x}) > 0$ for all $x \in [0, 1]$, the inverse mapping satisfies $DG(x) > 0$ for all $x \in [a, b]$. Therefore $b_2(\hat{x}) \ge c > 0 \ \forall\, \hat{x} \in [0, 1]$, and we can divide (3.36) by it and obtain

$$(\hat{D}^2 s_n)(\hat{\tau}_j) + \sum_{i=0}^{1} c_i(\hat{\tau}_j)(\hat{D}^i s_n)(\hat{\tau}_j) = \frac{1}{b_2(\hat{\tau}_j)}(D^2 v \circ F)(\hat{\tau}_j), \quad j = 1, 2. \tag{3.37}$$

The above problem can be written in the form

$$\hat{Q}_n(I + \hat{T})y_n = \hat{Q}_n \frac{(D^2 v) \circ F}{b_2}, \tag{3.38}$$

with $\hat{T} : C^0[0, 1] \to C^0[0, 1]$ a compact operator and $\hat{D}^2 s_n = y_n$, $s_n(0) = s_n(1) = 0$, by following the steps of Sec. 3.2.1.

By definition and by the same derivative transformation used above, we have

$$\begin{aligned} \|w_n\|_{L^\infty(a,b)} &= \|D^2 v_n\|_{L^\infty(a,b)} \\ &\simeq \left\| \hat{D}^2 s_n + \sum_{i=0}^{1} c_i(, \hat{D}^i s_n) \right\|_{L^\infty(0,1)} \\ &= \|(I + \hat{T})y_n\|_{L^\infty(0,1)}. \end{aligned} \tag{3.39}$$

A triangle inequality and the fact that $\hat{Q}_n y_n = y_n$, give

$$\|(I + \hat{T})y_n\|_{L^\infty(0,1)} \le \|(I + \hat{Q}_n \hat{T})y_n\|_{L^\infty(0,1)} + \|(I - \hat{Q}_n)\hat{T} y_n\|_{L^\infty(0,1)}. \tag{3.40}$$

Equation (3.38) and the stability of the spline interpolant $\hat{Q}_n$ yield immediately

$$\begin{aligned}\|(I+\hat{Q}_n\hat{T})y_n\|_{L^\infty(0,1)} &= \left\|\hat{Q}_n\frac{D^2v\circ F}{b_2}\right\|_{L^\infty(0,1)}\\ &\lesssim \left\|\frac{D^2v\circ F}{b_2}\right\|_{L^\infty(0,1)}\\ &\lesssim \|D^2v\|_{L^\infty(a,b)} = \|w\|_{L^\infty(a,b)}. \end{aligned} \tag{3.41}$$

Using the L^∞ stability of the interpolation operator $\hat{Q}_n$ and standard approximation properties for splines[14] it follows easily

$$\|(I-\hat{Q}_n)\psi\|_{L^\infty(0,1)} \lesssim c_n\|\psi\|_{W^{1,\infty}(0,1)} \quad \forall\,\psi\in W^{1,\infty}(0,1),$$

with $\lim_{n\to\infty} c_n = 0$. As a consequence, the second term in (3.40) can be bounded using the compactness of $\hat{T}$ and recalling (3.35). One gets

$$\begin{aligned}\|(I-\hat{Q}_n)\hat{T}y_n\|_{L^\infty(0,1)} &\lesssim c_n\|\hat{T}y_n\|_{W^{1,\infty}(0,1)} \lesssim c_n\|y_n\|_{L^\infty(0,1)}\\ &= c_n\|\hat{D}^2s_n\|_{L^\infty(0,1)} \lesssim c_n\|D^2v_n\|_{L^\infty(a,b)}\\ &= c_n\|w_n\|_{L^\infty(a,b)}. \end{aligned} \tag{3.42}$$

Combining (3.39) with (3.40)−(3.42) it follows that, for n sufficiently large,

$$\|w_n\|_{L^\infty(a,b)} \lesssim \|w\|_{L^\infty(a,b)}. \tag{3.43}$$

□

Combining the results of this section with Proposition 3.1 yields

Theorem 3.3. *Given a NURBS space $\mathcal{V}_{n+2}$ on $[a,b]$ and a set of collocation points $\{\tau_1,\dots,\tau_n\}\in[a,b]$, let the hypotheses of Theorem 3.2 on the collocation points and the spline space $\hat{\mathcal{S}}_{n+2}$ be satisfied. Then*

$$\|D^2(u-u_n)\|_{L^\infty[a,b]} \lesssim h^l\|u\|_{W^{l+2,\infty}[a,b]}, \tag{3.44}$$

where u is the solution of the continuous problem (3.16) and u_n is the solution of the collocation problem (3.25).

The NURBS collocation method is therefore optimal in the $W^{2,\infty}$ seminorm. The convergence in the full $W^{2,\infty}$ norm can be recovered using a Poincaré inequality

$$\|u-u_n\|_{W^{2,\infty}[a,b]} \lesssim h^l\|u\|_{W^{l+2,\infty}[a,b]}. \tag{3.45}$$

Therefore, in order to guarantee the optimal behavior of the collocation scheme (3.25), the collocation points can be selected according to Theorem 3.2. Notice that the space $\hat{\mathcal{T}}_n$, which is made of second derivatives of the splines in $\hat{\mathcal{S}}_{n+2}$, is still a space of splines. In particular, $\hat{\mathcal{T}}_n$ is the space of splines of degree $p-2$ on the knot vector obtained by removing the first two and last two knots from the knot vector of $\hat{\mathcal{S}}_{n+2}$. The optimal selection of points for interpolation of one-dimensional splines is addressed in various papers. The only choice which is proved to be stable for any mesh and degree is the one proposed by Demko.[15] These points are referred to as

Demko abscissae. They are the extrema of the Chebyshev splines, i.e. the splines that have the maximum number of oscillations, for which the extrema take the values ± 1. The Demko abscissae are obtained by an iterative algorithm (see, e.g. `chbpnt` in MATLAB and also the book by de Boor[14]). A different approach which is proposed in the engineering literature[23] is to collocate at the Greville abscissae. These are obtained as knots averages[14,15] (see (2.16)) and Greville abscissae interpolation is proved to be stable up to degree 3, while there are examples[24] of instability for degrees higher than 19 on particular non-uniform meshes.[a] In Sec. 4.1, we numerically test both possibilities, i.e. we consider:

- collocation at the images (though the geometry map F) of the Demko abscissae of the space $\hat{\mathcal{T}}_n$ (we refer to these as "second-derivative Demko abscissae");
- collocation at the images of the Greville abscissae of the space $\hat{\mathcal{S}}_{n+2}$, after removing the first and last knots (we refer to these as simply "Greville abscissae").

In both cases, boundary conditions will be imposed strongly on the discrete solution, according to formulation (3.25). It will be shown that the first choice (Demko abscissae) is superior, even though it represents a very small advantage over the second choice in many cases of practical interest.

In Fig. 2 we compare a sample of Demko abscissae for the space $\hat{\mathcal{T}}_n$, Greville abscissae for $\hat{\mathcal{T}}_n$, and Greville abscissae for $\hat{\mathcal{S}}_{n+2}$ after removing the first and last knots. We consider a uniform open knot vector with polynomial degree $p = 3$ in the first frame, with $p = 7$ in the second frame, and a non-uniform open knot vector with knot spans forming a geometric sequence with $p = 7$ in the last frame. Coordinates of collocation points are reported in Tables 1−3.

3.4. *Remarks on the theoretical analysis in higher dimensions*

The extension to the multi-dimensional case of the analysis of Sec. 3.2, based on the abstract framework of Sec. 3.1, poses various difficulties. One of the main issues is that the space consisting of the Laplacian of multivariate splines, or more generally of second-order derivatives of multivariate splines, is not a complete space of splines of a given degree. Therefore, stable interpolation in this space is difficult to determine. Thus, we only consider numerical experiments in Sec. 4.

Other approaches for the theoretical analysis of the collocation method with spline spaces in higher dimensions are given, for particular cases, in Arnold *et al.*[3] and Prenter.[26]

4. Numerical Tests

In this section we present some numerical results for the collocation approach proposed. We first study a one-dimensional second-order differential equation with

[a] To be precise, we refer to cases where the lengths of consecutive knot spans are increased by a constant scaling factor, forming a geometric sequence.

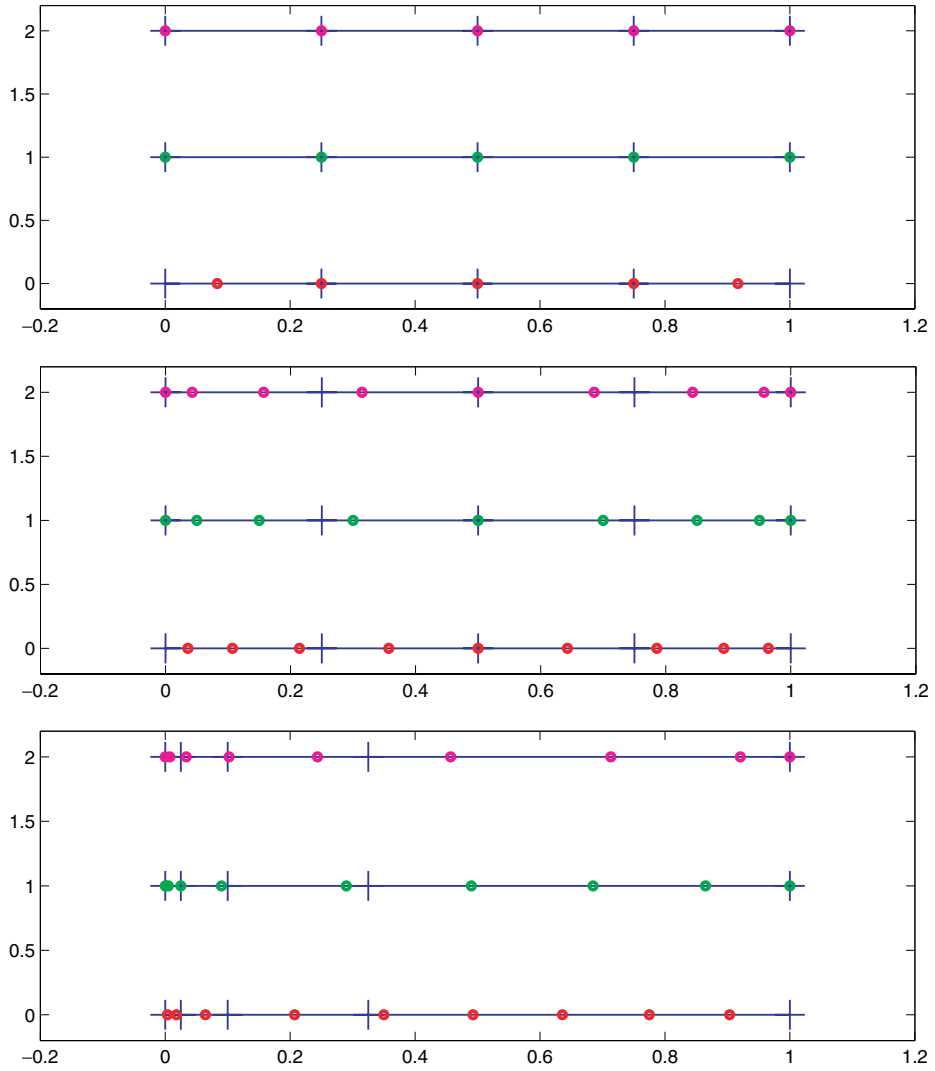

Fig. 2. Comparison of Demko abscissae for $\hat{\mathcal{T}}_n$ (first line of each frame), Greville abscissae for $\hat{\mathcal{T}}_n$ (second line), and Greville abscissae for $\hat{\mathcal{S}}_{n+2}$ after removing the first and last knots (third line). Uniform open knot vector with $p = 3$ (top frame), with $p = 7$ (middle frame), and non-uniform open knot vector with knot spans forming a geometric sequence with $p = 7$ (bottom frame).

Table 1. Coordinates of collocation points in Fig. 2 (upper frame): uniform mesh, $p = 3$.

Demko abscissae for $\hat{\mathcal{T}}_n$	0	0.2500	0.5000	0.7500	1.0000
Greville abscissae for $\hat{\mathcal{T}}_n$	0	0.2500	0.5000	0.7500	1.0000
Greville abscissae for $\hat{\mathcal{S}}_{n+2}$	0.0833	0.2500	0.5000	0.7500	0.9167

Table 2. Coordinates of collocation points in Fig. 2 (middle frame): uniform mesh, $p = 7$.

Demko abscissae for $\hat{\mathcal{T}}_n$	0	0.0429	0.1569	0.3144	0.5000	0.6856	0.8431	0.9571	1.0000
Greville abscissae for $\hat{\mathcal{T}}_n$	0	0.0500	0.1500	0.3000	0.5000	0.7000	0.8500	0.9500	1.0000
Greville abscissae for $\hat{\mathcal{S}}_{n+2}$	0.0357	0.1071	0.2143	0.3571	0.5000	0.6429	0.7857	0.8929	0.9643

Table 3. Coordinates of collocation points in Fig. 2 (bottom frame): knot spans forming a geometric sequence with $p = 7$.

Demko abscissae for $\hat{\mathcal{T}}_n$	0	0.0072	0.0336	0.1022	0.2438	0.4568	0.7134	0.9208	1.0000
Greville abscissae for $\hat{\mathcal{T}}_n$	0	0.0050	0.0250	0.0900	0.2900	0.4900	0.6850	0.8650	1.0000
Greville abscissae for $\hat{\mathcal{S}}_{n+2}$	0.0036	0.0179	0.0643	0.2071	0.3500	0.4929	0.6357	0.7750	0.9036

Dirichlet and Neumann boundary conditions, for linear and nonlinear parametrizations, either using Greville or second-derivative Demko abscissae (see Sec. 3.3). We also explore the 1D spectral approximation properties of the method. We then move to higher dimensions, focusing on an elliptic model problem defined on a quarter of an annulus in 2D and on a cube in 3D.

4.1. *One-dimensional source problem with Dirichlet boundary conditions*

The first test case we study is the following source problem defined on the domain $[0, 1]$:

$$\begin{cases} -u'' + u' + u = (1 + 4\pi^2)\sin(2\pi x) - 2\pi\cos(2\pi x), \quad \forall\, x \in (0, 1), \\ u(0) = u(1) = 0, \end{cases} \tag{4.1}$$

which admits the exact solution:

$$u = \sin(2\pi x). \tag{4.2}$$

This problem is numerically solved using the collocation method outlined in the previous sections, considering a linear parametrization ($F = \mathrm{Id}$) and employing both Greville and second-derivative Demko abscissae. In Figs. 3–5, we report log-scale plots of the relative errors for different degrees of approximations in L^∞-, $W^{1,\infty}$- and $W^{2,\infty}$-norms, respectively, for both choices of abscissae, recalling that

$$|\cdot|_{W^{i,\infty}} = \|D^i \cdot\|_{L^\infty}$$

and

$$\|\cdot\|_{W^{k,\infty}} = \sum_{i=0}^{k} \|D^i \cdot\|_{L^\infty}.$$

Denoting by p the degree of the approximation, the figures show that in the first two norms an order of convergence p is attained for even degrees, while an order $p - 1$ is attained for odd degrees. Instead in the $W^{2,\infty}$-norm, we observe the expected optimal

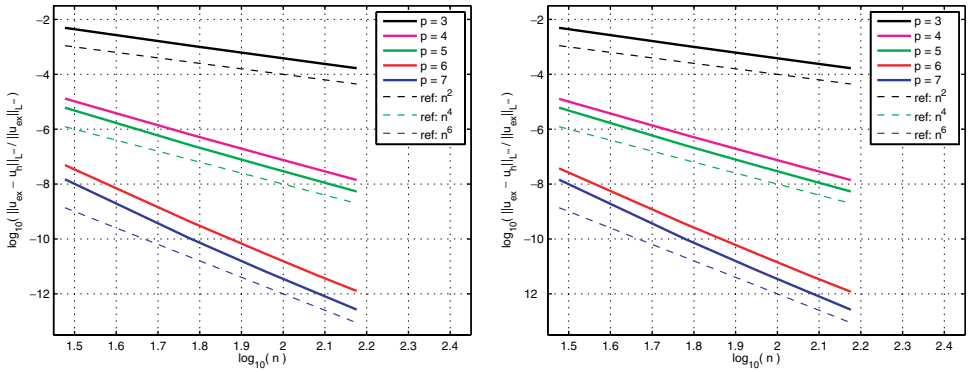

Fig. 3. 1D source problem with Dirichlet boundary conditions (linear parametrization), using Greville (left) and second-derivative Demko (right) abscissae. Relative error in L^∞-norm for different degrees of approximation.

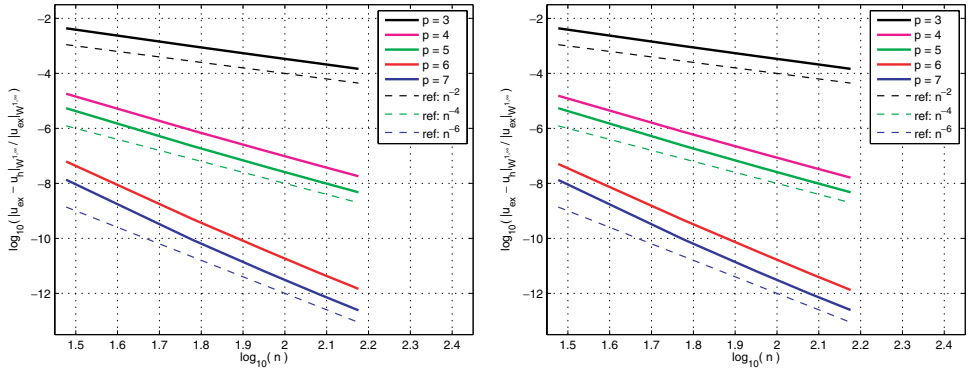

Fig. 4. 1D source problem with Dirichlet boundary conditions (linear parametrization), using Greville (left) and second-derivative Demko (right) abscissae. Relative error in $W^{1,\infty}$-norm for different degrees of approximation.

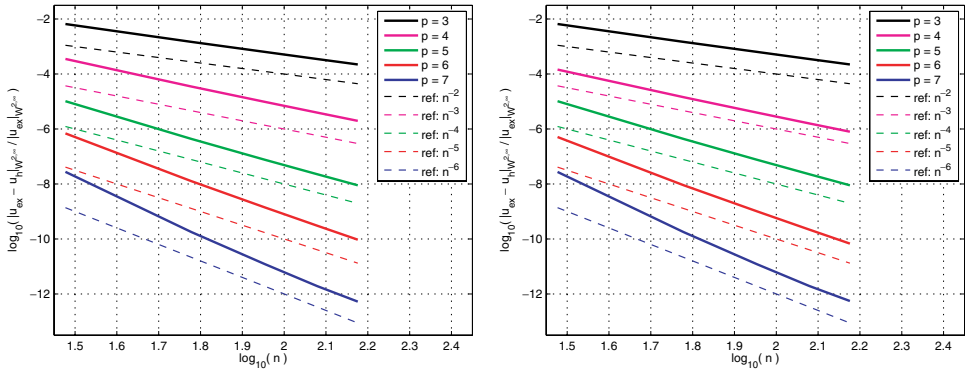

Fig. 5. 1D source problem with Dirichlet boundary conditions (linear parametrization), using Greville (left) and second-derivative Demko (right) abscissae. Relative error in $W^{2,\infty}$-norm for different degrees of approximation.

order of convergence, i.e. $p-1$, for all approximation degrees, in agreement with the predictions of the theory (see Sec. 3.3). Here, and in the following examples, the use of second-derivative Demko abscissae gives the same convergence rates as Greville, but a very slight difference in the magnitude of errors is observed for certain degrees.

We have not included results for $p=2$, since this case is not covered by the theory. However, the results obtained are in complete agreement with the ones observed for higher degrees (i.e. order p for the L^∞- and $W^{1,\infty}$-norms and $p-1$ for the $W^{2,\infty}$-norm).

As proven earlier, the optimal theoretical convergence rates are also expected when nonlinear parametrizations are employed, provided that the geometry map is kept fixed during the refinement process. In order to test this, we refer to a particular nonlinear mesh (an illustration of which is given in Fig. 6) and we solve the source problem with Dirichlet boundary conditions, using standard h-refinement procedures such that the geometry map is unchanged. The results are reported in Figs. 7–9 where it is possible to see the same orders of convergence observed in the case of linear parametrization. In particular, Fig. 9 shows how the $W^{2,\infty}$-norm errors converge with the expected optimal orders (i.e. $p-1$).

Finally, we consider a problem which shows a significant advantage in using second-derivative Demko abscissae, i.e. collocation points that guarantee optimal interpolation on the second derivatives of the discrete space. The differential equation is now

$$\begin{cases} u''(x) = f(x) \quad \forall\, x \in (0,1), \\ u(0) = u(1) = 0, \end{cases} \tag{4.3}$$

and, therefore, the collocation scheme is in fact reduced to a simple interpolation of second derivatives. We compare with the other two choices, i.e. collocation at Greville

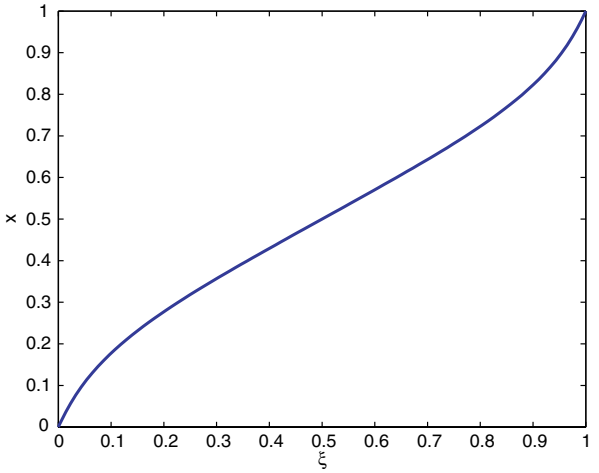

Fig. 6. Nonlinear geometry map.

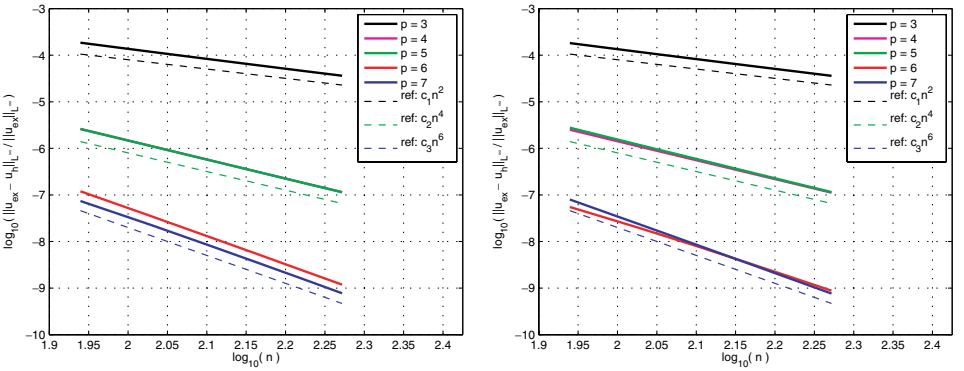

Fig. 7. 1D source problem with Dirichlet boundary conditions (nonlinear parametrization of Fig. 6), using Greville (left) and second-derivative Demko (right) abscissae. Relative error in L^∞-norm for different degrees of approximation.

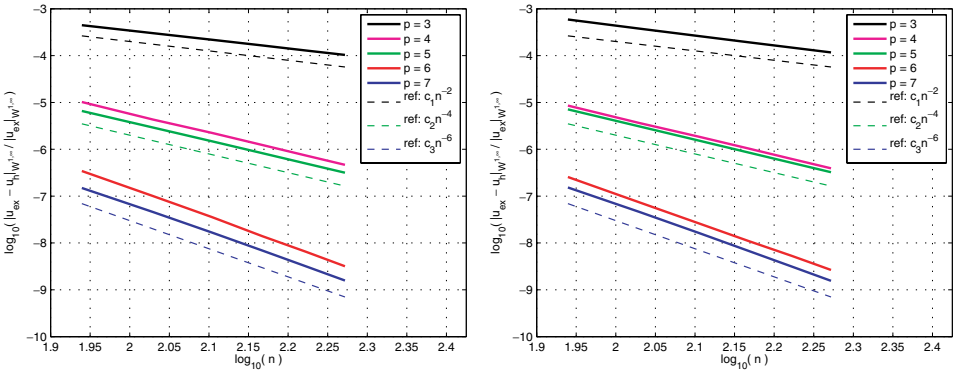

Fig. 8. 1D source problem with Dirichlet boundary conditions (nonlinear parametrization of Fig. 6), using Greville (left) and second-derivative Demko (right) abscissae. Relative error in $W^{1,\infty}$-norm for different degrees of approximation.

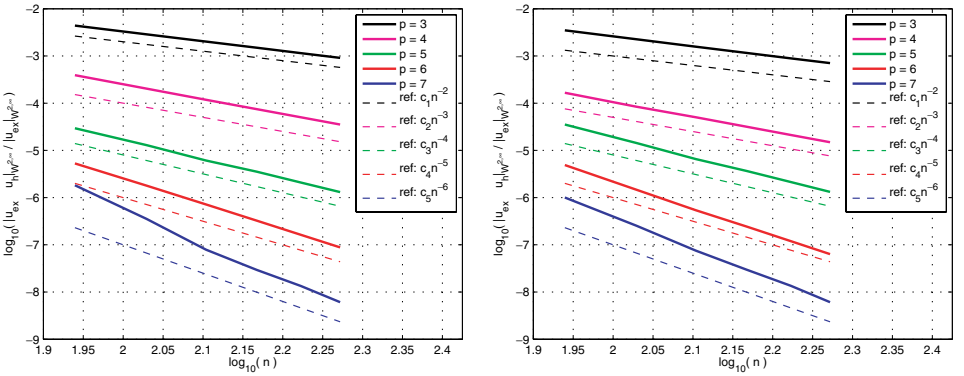

Fig. 9. 1D source problem with Dirichlet boundary conditions (nonlinear parametrization of Fig. 6), using Greville (left) and second-derivative Demko (right) abscissae. Relative error in $W^{2,\infty}$-norm for different degrees of approximation.

abscissae for the space of unknown functions or for the space of second derivatives, respectively. The unknown is sought in the space of splines of degree $p = 7$ (with C^6 continuity) and a linear geometrical parametrization $F : [0, 1] \to [0, 1]$ is adopted. The right-hand side is selected to give the exact solution $u(x) = x^{2.01}(1 - x)$, whose second derivative presents a thin layer at $x = 0$. On $[0, 1]$ we consider a geometrically graded mesh, where the ratio between adjacent element (i.e. knot span) lengths is 3. In Fig. 10, the error in the $W^{2,\infty}$-norm versus the number of elements of the mesh is plotted. It can be seen how in some pathological cases collocation at the second-derivative Demko abscissae may lead to higher accuracy whereas Greville abscissae fail to converge. We also observe that collocation at Greville abscissae is more accurate if one computes them on the space of second derivatives.

4.2. *One-dimensional source problem with Dirichlet–Neumann boundary conditions*

We now study a source problem similar to problem (4.1), but here a Neumann boundary condition is imposed at the second end of the domain. Namely, the differential problem to be solved is

$$\begin{cases} -u'' + u' + u = (1 + 4\pi^2)\cos(2\pi x) - 2\pi \sin(2\pi x) - 1, \quad \forall\, x \in (0, 1), \\ u(0) = u'(1) = 0, \end{cases} \tag{4.4}$$

which admits the exact solution:

$$u = \cos(2\pi x) - 1. \tag{4.5}$$

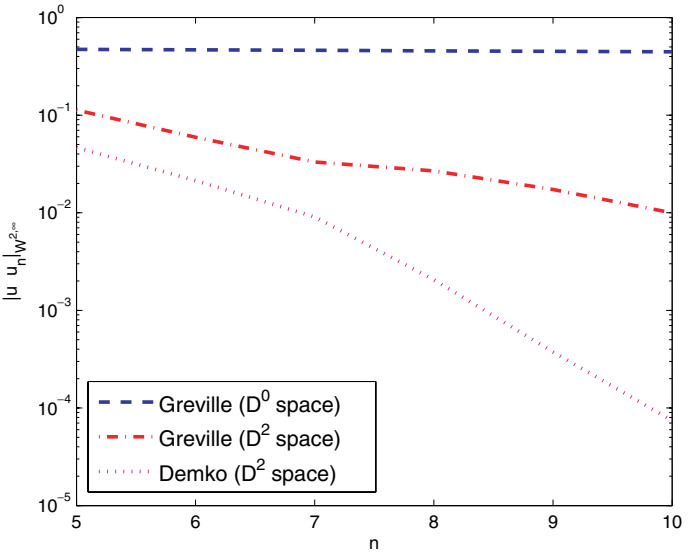

Fig. 10. Comparison of different choices of collocation points for $p = 7$ and a geometrically graded mesh: Greville abscissae for the space of unknowns; Greville abscissae for the space of second derivatives; and Demko abscissae for the space of second derivatives.

Again, the problem is numerically solved considering a linear parametrization and employing collocation methods based on both Greville and second-derivative Demko abscissae. The results are then reported in Figs. 11−13 where it is possible to see the same orders of convergence observed in the case of Dirichlet boundary conditions. In particular, Fig. 13 shows how the $W^{2,\infty}$-norm errors converge with the expected optimal orders (i.e. $p-1$).

4.3. *One-dimensional eigenvalue problem*

We now study the following eigenvalue problem

$$\begin{cases} u'' + \omega^2 u = 0, & \forall\, x \in (0,1), \\ u(0) = u(1) = 0, \end{cases} \tag{4.6}$$

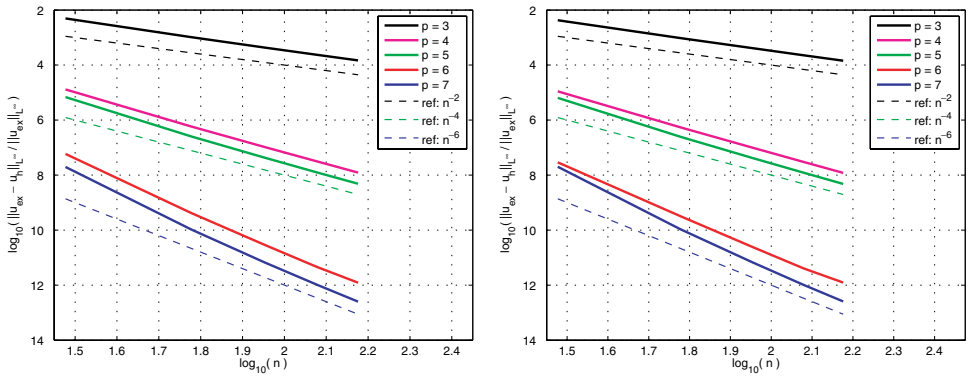

Fig. 11. 1D source problem with Dirichlet−Neumann boundary conditions (linear parametrization), using Greville (left) and second-derivative Demko (right) abscissae. Relative error in L^∞-norm for different degrees of approximation.

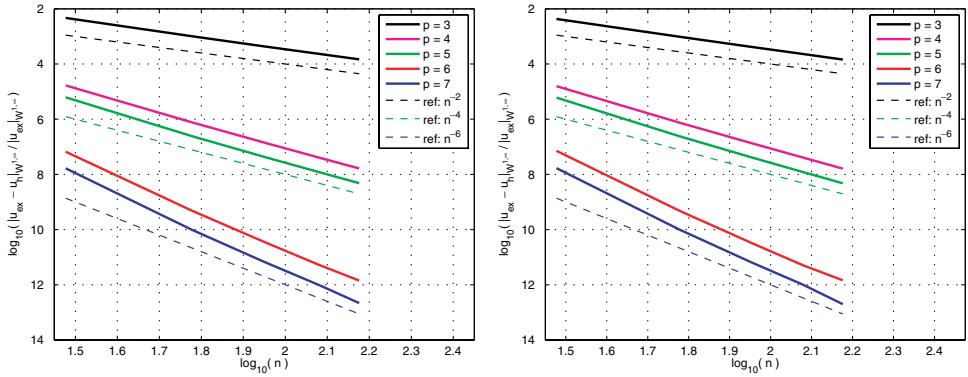

Fig. 12. 1D source problem with Dirichlet−Neumann boundary conditions (linear parametrization), using Greville (left) and second-derivative Demko (right) abscissae. Relative error in $W^{1,\infty}$-norm for different degrees of approximation.

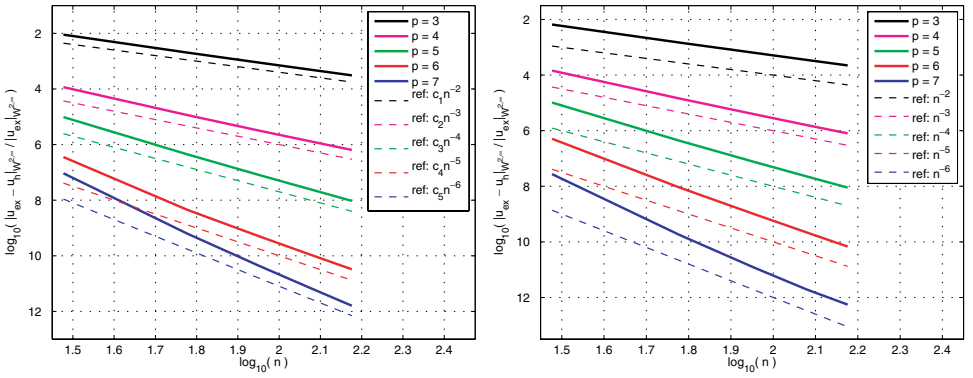

Fig. 13. 1D source problem with Dirichlet−Neumann boundary conditions (linear parametrization), using Greville (left) and second-derivative Demko (right) abscissae. Relative error in $W^{2,\infty}$-norm for different degrees of approximation.

for which the exact frequencies ω_n are given by:

$$\omega_n = 2\pi n, \quad \text{with } n = 1, 2, 3, \dots. \tag{4.7}$$

This problem can also be solved using the collocation method with both Greville and second-derivative Demko abscissae. In Fig. 14, we plot the results in terms of normalized discrete spectra, obtained considering a linear parametrization and using different degrees of approximation (1000 d.o.f.'s have been used to produce each spectrum). It is possible to observe the good behavior of all spectra, which converge for an increasing degree p. In Figs. 15 and 16, we also report the convergence plot of the first three eigenvalues for $p = 3$ and $p = 4$, respectively. It is possible to observe that the order of convergence is in all cases $2(p - 2)$.

We note that in this case "outlier frequencies" appear at the very end of the spectrum (the maximum outlier being almost double the corresponding exact frequency). This behavior is analogous to the one of Galerkin-based isogeometric discretization[11,20]

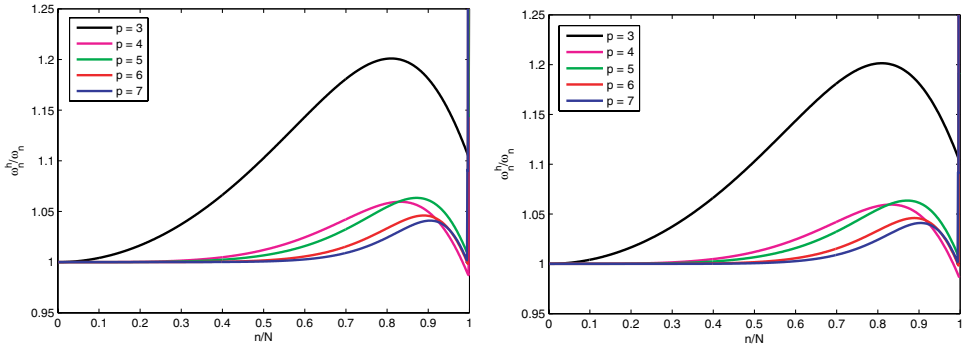

Fig. 14. 1D eigenvalue problem with linear parametrization using Greville (left) and second-derivative Demko (right) abscissae. Normalized spectra for different degrees of approximation.

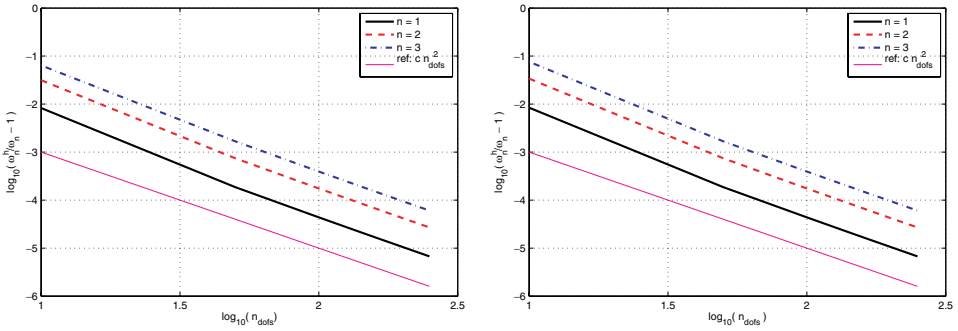

Fig. 15. 1D eigenvalue problem with linear parametrization using Greville (left) and second-derivative Demko (right) abscissae. Convergence of the first three eigenvalues for $p = 3$.

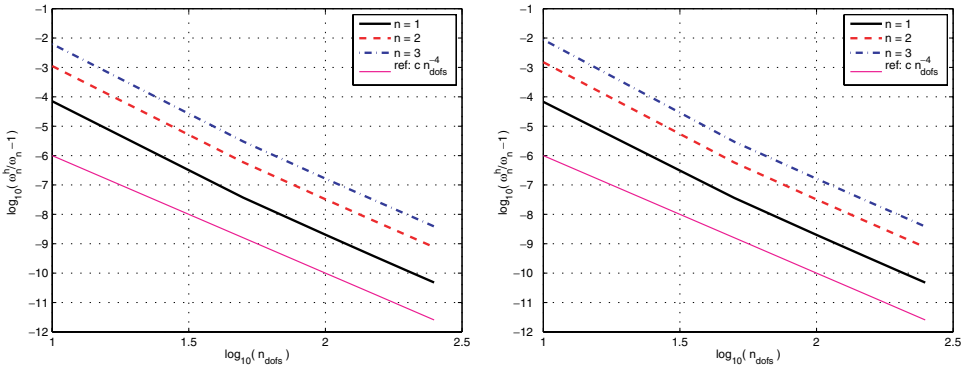

Fig. 16. 1D eigenvalue problem with linear parametrization using Greville (left) and second-derivative Demko (right) abscissae. Convergence of the first three eigenvalues for $p = 4$.

and can be circumvented resorting to a suitable nonlinear parametrization of the domain obtained by a uniform control mesh[20] for more details). In Fig. 17 we report the normalized discrete spectra obtained using the nonlinear parametrization, which appear to be identical to those for a linear parametrization except that outliers are eliminated.

4.4. *Two-dimensional source problem*

We now consider higher-dimensional problems and we start with the solution of an elliptic model problem on a 2D domain Ω consisting of a quarter of an annulus, as sketched in Fig. 18. Here we select internal and external radii equal to $R_1 = 1$ and $R_2 = 4$, respectively. Moreover, we insert a C^1-continuous central circumferential line, in order to test the method behavior also in case of reduced continuity. Such a domain can be exactly represented by a single NURBS patch, as shown in Fig. 19, where we illustrate the control mesh, knot lines, and Greville abscissae using quartic

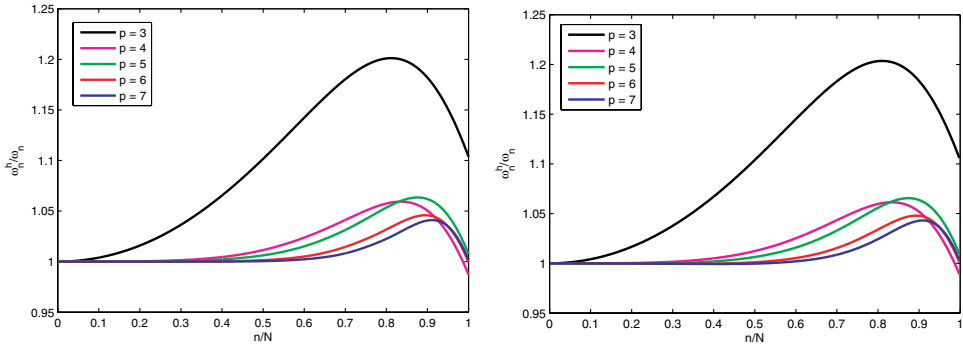

Fig. 17. 1D eigenvalue problem for a uniform control mesh (i.e. nonlinear parametrization) using Greville (left) and second-derivative Demko (right) abscissae. Normalized spectra for different degrees of approximation.

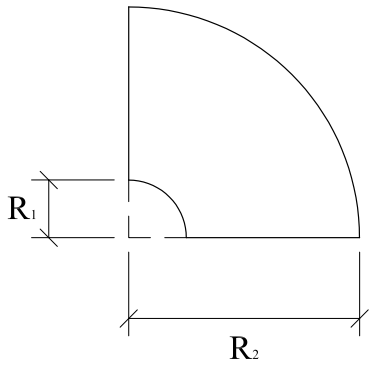

Fig. 18. Geometry for the quarter of an annulus.

NURBS and 8×10 control points (note that in the plot we do not report Greville abscissae collocated on the domain boundary). The knot vectors, control points, weights, and Greville abscissae employed for the example of Fig. 19 are reported in Table 4.

The problem to be solved reads

$$\begin{cases} -\triangle u + u = f, & \forall\, x \in \Omega, \\ u|_{\partial\Omega} = 0, \end{cases} \tag{4.8}$$

with

$$\begin{aligned} f = {} & (3x^4 - 67x^2 - 67y^2 + 3y^4 + 6x^2y^2 + 116)\sin(x)\sin(y) \\ & + (68x - 8x^3 - 8xy^2)\cos(x)\sin(y) \\ & + (68y - 8y^3 - 8yx^2)\cos(y)\sin(x), \end{aligned} \tag{4.9}$$

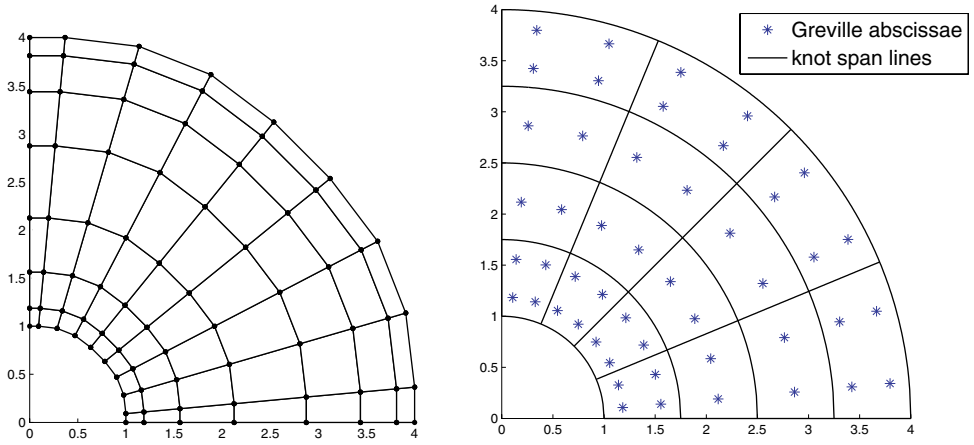

Fig. 19. Quarter of an annulus: control mesh (left) and knot lines and locations of interior Greville abscissae (right) in the case of quartic NURBS with 8×10 control points. There are 32 additional Greville abscissae on the boundary of the domain (not shown).

such that the exact solution is

$$u = (x^2 + y^2 - 1)(x^2 + y^2 - 16)\sin(x)\sin(y). \tag{4.10}$$

In Fig. 20, we present the results obtained employing Greville abscissae (in the $W^{2,\infty}$-norm, which is the one for which we have theoretical results in 1D). It is possible to observe that, even though for higher-dimensional cases we have no mathematical theory, the same orders of convergence in the $W^{2,\infty}$-norm expected in 1D (i.e. $p - 1$) are attained also in 2D. Notice that the plot abscissa is the square root of the total number of control points used.

4.5. *Three-dimensional source problem*

We then study an elliptic model problem on the 3D cubic domain $[0, 1] \times [0, 1] \times [0, 1]$, i.e.

$$\begin{cases} -\triangle u + u = f, & \forall\, x \in [0,1] \times [0,1] \times [0,1], \\ u|_{\partial\Omega} = 0, \end{cases} \tag{4.11}$$

with

$$f = (1 + 12\pi^2)\sin(2\pi x)\sin(2\pi y)\sin(2\pi z),$$

such that the exact solution is

$$u = \sin(2\pi x)\sin(2\pi y)\sin(2\pi z). \tag{4.12}$$

In Fig. 21, we present the results obtained (in the $W^{2,\infty}$-norm) employing Greville abscissae. The same orders of convergence in the $W^{2,\infty}$-norm expected in the 1D case (i.e. $p - 1$) are attained (notice that the plot abscissa is the cube root of the total

Table 4. Knot vectors, control points, weights, and Greville abscissae employed for the example of Fig. 19.

Knot vectors	
ξ-direction (radial)	{0, 0, 0, 0, 0, 1/4, 1/2, 1/2, 1/2, 3/4, 1, 1, 1, 1, 1}
η-direction (circumf.)	{0, 0, 0, 0, 0, 1/4, 1/2, 3/4, 1, 1, 1, 1, 1}

Control points, weights, and Greville abscissae

Control points and weights			Greville abscissae		Control points and weights			Greville abscissae	
x-coord.	y-coord.	weight	x-coord.	y-coord.	x-coord.	y-coord.	weight	x-coord.	y-coord.
1.0000	0.0000	1.0000	1.0000	0.0000	2.8750	0.0000	1.0000	2.8750	0.0000
1.0000	0.0917	0.9634	0.9960	0.0899	2.8750	0.2638	0.9634	2.8634	0.2583
0.9769	0.2843	0.9024	0.9614	0.2752	2.8086	0.8173	0.9024	2.7640	0.7911
0.9037	0.4706	0.8658	0.8883	0.4593	2.5983	1.3530	0.8658	2.5538	1.3205
0.7803	0.6339	0.8536	0.7764	0.6303	2.2434	1.8224	0.8536	2.2320	1.8121
0.6339	0.7803	0.8536	0.6303	0.7764	1.8224	2.2434	0.8536	1.8121	2.2320
0.4706	0.9037	0.8658	0.4593	0.8883	1.3530	2.5983	0.8658	1.3205	2.5538
0.2843	0.9769	0.9024	0.2752	0.9614	0.8173	2.8086	0.9024	0.7911	2.7640
0.0917	1.0000	0.9634	0.0899	0.9960	0.2638	2.8750	0.9634	0.2583	2.8634
0.0000	1.0000	1.0000	0.0000	1.0000	0.0000	2.8750	1.0000	0.0000	2.8750
1.1875	0.0000	1.0000	1.1875	0.0000	3.4375	0.0000	1.0000	3.4375	0.0000
1.1875	0.1090	0.9634	1.1827	0.1067	3.4375	0.3154	0.9634	3.4236	0.3089
1.1601	0.3376	0.9024	1.1417	0.3268	3.3581	0.9773	0.9024	3.3048	0.9459
1.0732	0.5588	0.8658	1.0548	0.5454	3.1066	1.6177	0.8658	3.0535	1.5788
0.9266	0.7527	0.8536	0.9219	0.7485	2.6824	2.1790	0.8536	2.6687	2.1666
0.7527	0.9266	0.8536	0.7485	0.9219	2.1790	2.6824	0.8536	2.1666	2.6687
0.5588	1.0732	0.8658	0.5454	1.0548	1.6177	3.1066	0.8658	1.5788	3.0535
0.3376	1.1601	0.9024	0.3268	1.1417	0.9773	3.3581	0.9024	0.9459	3.3048
0.1090	1.1875	0.9634	0.1067	1.1827	0.3154	3.4375	0.9634	0.3089	3.4236
0.0000	1.1875	1.0000	0.0000	1.1875	0.0000	3.4375	1.0000	0.0000	3.4375
1.5625	0.0000	1.0000	1.5625	0.0000	3.8125	0.0000	1.0000	3.8125	0.0000
1.5625	0.1434	0.9634	1.5562	0.1404	3.8125	0.3498	0.9634	3.7971	0.3426
1.5264	0.4442	0.9024	1.5022	0.4299	3.7245	1.0839	0.9024	3.6653	1.0490
1.4121	0.7353	0.8658	1.3879	0.7176	3.4455	1.7942	0.8658	3.3866	1.7511
1.2193	0.9904	0.8536	1.2131	0.9848	2.9750	2.4167	0.8536	2.9598	2.4030
0.9904	1.2193	0.8536	0.9848	1.2131	2.4167	2.9750	0.8536	2.4030	2.9598
0.7353	1.4121	0.8658	0.7176	1.3879	1.7942	3.4455	0.8658	1.7511	3.3866
0.4442	1.5264	0.9024	0.4299	1.5022	1.0839	3.7245	0.9024	1.0490	3.6653
0.1434	1.5625	0.9634	0.1404	1.5562	0.3498	3.8125	0.9634	0.3426	3.7971
0.0000	1.5625	1.0000	0.0000	1.5625	0.0000	3.8125	1.0000	0.0000	3.8125
2.1250	0.0000	1.0000	2.1250	0.0000	4.0000	0.0000	1.0000	4.0000	0.0000
2.1250	0.1950	0.9634	2.1164	0.1909	4.0000	0.3670	0.9634	3.9838	0.3594
2.0759	0.6041	0.9024	2.0430	0.5847	3.9077	1.1372	0.9024	3.8456	1.1006
1.9205	1.0000	0.8658	1.8876	0.9760	3.6150	1.8824	0.8658	3.5531	1.8372
1.6582	1.3470	0.8536	1.6498	1.3394	3.1213	2.5355	0.8536	3.1054	2.5212
1.3470	1.6582	0.8536	1.3394	1.6498	2.5355	3.1213	0.8536	2.5212	3.1054
1.0000	1.9205	0.8658	0.9760	1.8876	1.8824	3.6150	0.8658	1.8372	3.5531
0.6041	2.0759	0.9024	0.5847	2.0430	1.1372	3.9077	0.9024	1.1006	3.8456
0.1950	2.1250	0.9634	0.1909	2.1164	0.3670	4.0000	0.9634	0.3594	3.9838
0.0000	2.1250	1.0000	0.0000	2.1250	0.0000	4.0000	1.0000	0.0000	4.0000

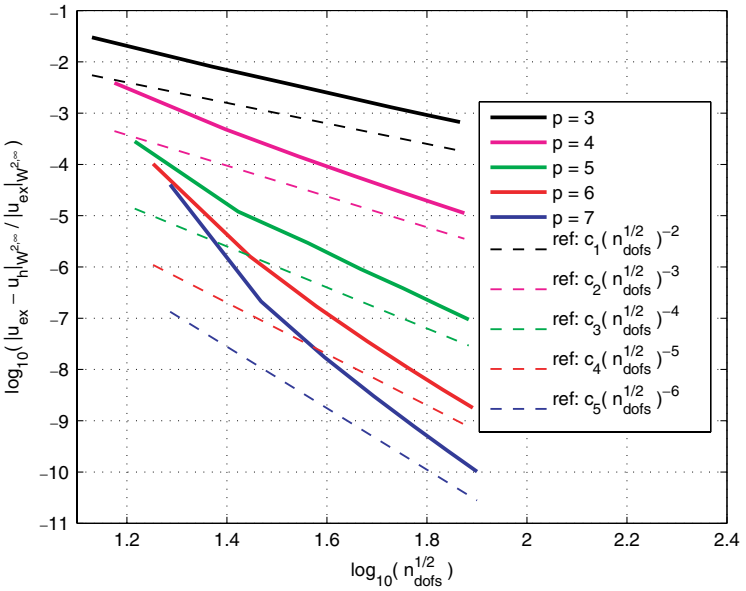

Fig. 20. 2D elliptic model problem on a quarter of an annulus, using Greville abscissae. Relative error in $W^{2,\infty}$-norm for different degrees of approximation.

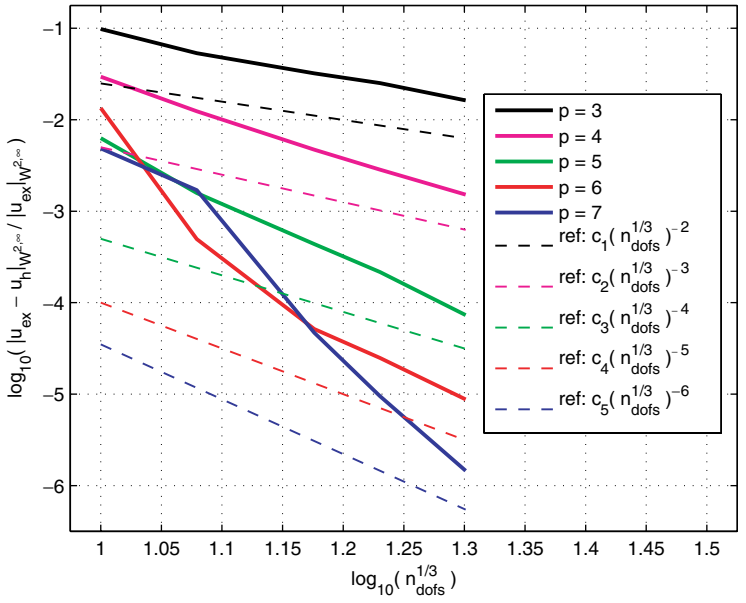

Fig. 21. 3D elliptic model problem on a cube, using Greville abscissae. Relative error in $W^{2,\infty}$-norm for different degrees of approximation.

Table 5. Order with respect to the bandwidth b, for collocation and Galerkin-based isogeometric analysis.

	Collocation; p odd	Collocation; p even	Galerkin
$\|u - u_n\|_{L^\infty}$	$O(h^{b-1})$		$O(h^{(b+1)/2})$
$\|u - u_n\|_{W^{1,\infty}}$	$O(h^{b-1})$		$O(h^{(b-1)/2})$
$\|u - u_n\|_{W^{2,\infty}}$	$O(h^{b-1})$	$O(h^{b-2})$	$O(h^{(b-3)/2})$
Eigenvalues	$O(h^{2b-4})$	$O(h^{2b-6})$	$O(h^{b-1})$

number of control points used, i.e., in this case, the number of control points per direction).

5. Discussion of the Computational Cost

This section is devoted to an analysis of the computational cost of the isogeometric collocation approach, comparing with the Galerkin version of isogeometric analysis.

In the previous sections, we have analyzed the accuracy of the method as a function of the mesh-size h and the order p. Given h and p, isogeometric collocation is less than or equal in accuracy to the Galerkin isogeometric method. However, it is clear that this comparison does not properly account for computational cost. A meaningful comparison between the two methods is not simple. Nevertheless, we will attempt to provide some initial insights by comparing two aspects: initial formation of the equation system and its solution.

Forming the system of equations is where collocation has a great advantage over the Galerkin method: the number of evaluations required is equal to the number of control points for collocation, while the integrals of a Galerkin formulation need rules that use a number of quadrature points in each element proportional to p, that is $p + 1$ for Gaussian or approximately $p/2$ for the rules proposed by Hughes *et al.*[21]

The computational cost for solving the system of equations is a more complex issue. Following Kwok *et al.*,[22] we take the view that the bandwidth of the matrices is the indicator of the computational cost, so methods with the same bandwidth are compared. We consider the one-dimensional case, and a uniform mesh in the parametric interval $(0, 1)$. In this case, the bandwidth of the collocation method is $b = p$ or $b = p + 1$ for p odd or even, respectively. For the Galerkin method, the bandwidth is $2p + 1$, for all p. The order of convergence with respect to the bandwidth is summarized in Table 5. For the collocation method, the orders are obtained from the numerical tests of Sec. 4.1, supported by the theoretical analysis of Sec. 3.2. For source problems, collocation is always advantageous, while for eigenvalue problems collocation is advantageous for p odd and the advantage also holds for p even when $b \geq 5$.

6. Conclusions

In the finite element method, the Galerkin, and related formulations have dominated. Collocation has been investigated but has seemed to offer little theoretical advantage

and no practical usefulness. Our view is that the reason for this is that most finite element procedures utilize functions which are no more than C^0-continuous. This lack of smoothness eliminates the possibility of developing methods based on the strong form of differential equations. Some C^1-continuous finite elements in two dimensions have been developed but their use has also been very limited because of their complexity and other practical requirements.

Isogeometric analysis, on the other hand, presents an opportunity because it is possible to generate smoother basis functions for geometrically and topologically complex domains. Thus, collocation becomes feasible, while retaining the attributes of isogeometric analysis and in particular the possible direct link with CAD generated geometry. The major advantage of collocation is the reduced number of evaluation points compared with the Galerkin method. Analysis methodology dominated by the cost of quadrature would seem to benefit most from collocation. A specific example that may be mentioned in this regard is explicit transient analysis.[18]

Effective isogeometric collocation methods depend on the stability of the discrete equation system and the ability to generate smooth basis functions (at least C^1) for complex objects. Much progress has been made on this latter topic in recent years, but it is mostly focused on surfaces rather than 3D solids. The 3D problem may still be considered an open problem. There is much additional research necessary to make collocation methods a practical reality for engineering analysis. However, we believe the door is now open and the potential benefits may be significant.

Acknowledgments

L. Beirão da Veiga, A. Reali and G. Sangalli were partially supported by the European Research Council through the FP7 Ideas Starting Grant 205004: *GeoPDEs — Innovative compatible discretization techniques for Partial Differential Equations.* T. J. R. Hughes was partially supported by Office of Naval Research Contracts N00014-03-1-0263 and N00014-08-1-0992. This support is gratefully acknowledged.

References

1. I. Akkermann, Y. Bazilevs, V. M. Calo, T. J. R. Hughes and S. Hulshoff, The role of continuity in residual-based variational multiscale modeling of turbulence, *Comput. Mech.* **41** (2008) 371−378.
2. D. N. Arnold and W. L. Wendland, On the asymptotic convergence of collocation methods, *Math. Comput.* **41** (1983) 349−381.
3. D. N. Arnold and J. Saranen, On the asymptotic convergence of spline collocation methods for partial differential equations, *SIAM J. Numer. Anal.* **21** (1984) 459−472.
4. F. Auricchio, L. Beirão da Veiga, A. Buffa, C. Lovadina, A. Reali and G. Sangalli, A fully "locking-free" isogeometric approach for plane linear elasticity problems: A stream function formulation, *Comput. Methods Appl. Mech. Engrg.* **197** (2007) 160−172.
5. F. Auricchio, L. Beirão da Veiga, C. Lovadina and A. Reali, The importance of the exact satisfaction of the incompressibility constraint in nonlinear elasticity: Mixed FEMs versus

NURBS-based approximations, *Comput. Methods Appl. Mech. Engrg.*, doi:10.1016/j.cma.2008.06.004.
6. Y. Bazilevs, L. Beirão da Veiga, J. A. Cottrell, T. J. R. Hughes and G. Sangalli, Isogeometric analysis: Approximation, stability and error estimates for h-refined meshes, *Math. Models Methods Appl. Sci.* **16** (2006) 1–60.
7. Y. Bazilevs, C. Michler, V. M. Calo and T. J. R. Hughes, Weak Dirichlet boundary conditions for wall-bounded turbulent flows, *Comput. Methods Appl. Mech. Engrg.* **196** (2007) 4853–4862.
8. Y. Bazilevs, V. M. Calo, J. A. Cottrell, T. J. R. Hughes, A. Reali and G. Scovazzi, Variational multiscale residual-based turbulence modeling for large eddy simulation of incompressible flows, *Comput. Methods Appl. Mech. Engrg.* **197** (2007) 173–201.
9. L. Beirão da Veiga, A. Buffa, J. Rivas and G. Sangalli, Some estimates for $h-p-k$-refinement in isogeometric analysis, Tech. Rep., IMATI-CNR, 2009.
10. J. A. Cottrell, T. J. R. Hughes and Y. Bazilevs, *Isogeometric Analysis. Towards Integration of CAD and FEA* (Wiley, 2009).
11. J. A. Cottrell, A. Reali, Y. Bazilevs and T. J. R. Hughes, Isogeometric analysis of structural vibrations, *Comput. Methods Appl. Mech. Engrg.* **195** (2006) 5257–5296.
12. J. A. Cottrell, T. J. R. Hughes and A. Reali, Studies of refinement and continuity in isogeometric structural analysis, *Comput. Methods Appl. Mech. Engrg.* **196** (2007) 4160–4183.
13. C. de Boor and B. Swartz, Collocation at Gaussian points, *SIAM J. Numer. Anal.* **10** (1973) 582–606.
14. C. de Boor, A practical guide to splines, *SIAM J. Numer. Anal.* **10** (1973) 582–606.
15. S. Demko, On the existence of interpolation projectors onto spline spaces, *J. Approx. Theory* **43** (1985) 151–156.
16. M. R. Dörfel, B. Jüttler and B. Simeon, Adaptive isogeometric analysis by local h-refinement with T-splines, *Comput. Methods Appl. Mech. Engrg.*, in press.
17. G. E. Farin, *NURBS Curves and Surfaces*: *From Projective Geometry to Practical Use* (A. K. Peters, 1995).
18. T. J. R. Hughes, *The Finite Element Method*: *Linear Static and Dynamic Finite Element Anal.* (Dover Publications, 2000).
19. T. J. R. Hughes, J. A. Cottrell and Y. Bazilevs, Isogeometric analysis: CAD, finite elements, NURBS, exact geometry, and mesh refinement, *Comput. Methods Appl. Mech. Engrg.* **194** (2005) 4135–4195.
20. T. J. R. Hughes, A. Reali and G. Sangalli, Duality and unified analysis of discrete approximations in structural dynamics and wave propagation: Comparison of p-method finite elements with k-method NURBS, *Comput. Methods Appl. Mech. Engrg.* **197** (2008) 4104–4124.
21. T. J. R. Hughes, A. Reali and G. Sangalli, Efficient quadrature for NURBS-based isogeometric analysis, *Comput. Methods Appl. Mech. Engrg.*, doi:10.1016/j.cma.2008.12.004.
22. Y. Kwok, R. D. Moser and J. Jimenez, A critical evaluation of the resolution properties of B-spline and compact finite difference methods, *J. Comput. Phys.* **174** (2001) 510–551.
23. R. W. Johnson, A B-spline collocation method for solving the incompressible Navier–Stokes equations using an *ad hoc* method: The boundary residual method, *Comput. Fluids* **34** (2005) 121–149.
24. R. Q. Jia, Spline interpolation at knot averages, *Constr. Approx.* **4** (1988) 1–7.
25. L. Piegl and W. Tiller, *The NURBS Book*, 2nd edn. (Springer-Verlag, 1997).
26. P. M. Prenter, *Splines and Variational Methods* (Wiley, 1989).

27. A. Reali, An isogeometric analysis approach for the study of structural vibrations, *J. Earthquake Engrg.* **10** (2006) 1−30.
28. D. F. Rogers, *An Introduction to NURBS with Historical Perspective* (Academic Press, 2001).
29. L. L. Schumaker, *Spline Functions*: *Basic Theory* (Krieger, 1993).
30. Y. Zhang, Y. Bazilevs, S. Goswami, C. L. Bajaj and T. J. R. Hughes, Patient-specific vascular NURBS modeling for isogeometric analysis of blood flow, *Comput. Methods Appl. Mech. Engrg.* **196** (2007) 2943−2959.